

Structural change and phase coexistence upon magnetic ordering in the magnetodielectric spinel Mn_3O_4

Moureen C. Kemei,^{*} Jaye K. Harada,[†] and Ram Seshadri[‡]
*Materials Department and Materials Research Laboratory
University of California, Santa Barbara, CA, 93106, USA*

Matthew R. Suchomel[§]
*X-Ray Science Division and Material Science Division
Argonne National Laboratory, Argonne IL, 60439, USA*
(Dated: July 10, 2014)

Cooperative Jahn-Teller ordering is well-known to drive the cubic $Fd\bar{3}m$ to tetragonal $I4_1/amd$ structural distortion in Mn_3O_4 at 1170 °C. Further structural distortion occurs in Mn_3O_4 upon magnetic ordering at 42 K. Employing high-resolution variable-temperature synchrotron x-ray diffraction we show that tetragonal $I4_1/amd$ and orthorhombic $Fddd$ phases coexist, with nearly equal fractions, below the Néel temperature of Mn_3O_4 . Significant variation of the orthorhombic a and b lattice constants from the tetragonal a lattice constant is observed. Structural phase coexistence in Mn_3O_4 is attributed to large strains due to the lattice mismatch between the tetragonal $I4_1/amd$ and the orthorhombic $Fddd$ phases. Strain tensors determined from Rietveld refinement show a highly strained matrix of the $I4_1/amd$ phase that accommodates the nucleated orthorhombic $Fddd$ phase in the phase coexistence regime. A comparison of the deformation observed in Mn_3O_4 to structural deformations of other magnetic spinels shows that phase coexistence may be a common theme when structural distortions occur below 50 K.

PACS numbers: 75.47.Lx, 75.50.Gg, 61.50.Ks

I. INTRODUCTION

Phase coexistence is a recurring theme that has been extensively investigated in perovskite manganese oxides displaying colossal magnetoresistance.¹ Phase separation of charge ordered insulating (antiferromagnetic) and metallic (ferromagnetic) phases has been observed in the manganites $(\text{La,Pr,Ca})\text{MnO}_3$.^{2,3} Competing double exchange mechanisms and Jahn-Teller-like electron-lattice coupling have been proposed to explain the coexistence of multiple phases.^{2,3} Chemical disorder has also been invoked to explain microscale structural phase separation.^{4,5} However, generalizations in describing the mechanisms of phase coexistence are often insufficient in describing all aspects of these phenomena prompting continued interest in these materials.⁶ Here, we encounter structural phase coexistence below the Néel temperature of the spinel Mn_3O_4 .

Mn_3O_4 (the mineral hausmanite) consists of edge sharing MnO_6 octahedra that are corner connected to MnO_4 tetrahedra. It is a cubic spinel in the space group $Fd\bar{3}m$ above 1170 °C. Mn_3O_4 undergoes a cooperative Jahn-Teller distortion below 1170 °C due to orbital degeneracy of the e_g^1 states of Mn^{3+} cations that occupy the octahedral sites. Jahn-Teller ordering of the octahedral e_g states stabilizes the z^2 orbital by elongating the MnO_6 octahedral units resulting in tetragonal $I4_1/amd$ symmetry below 1170 °C.^{7,8} Mn_3O_4 is a paramagnet above the Néel temperature (T_N) = 41 K, below T_N , it adopts a non-collinear magnetic structure that consists of ferromagnetically coupled Mn^{2+} cations along the (010) direction and two Mn^{3+} sub-lattices with a net moment

that couples antiferromagnetically to the magnetization of Mn^{2+} cations. A transition to an incommensurate spiral configuration occurs at 39 K, followed by a transition to commensurate spiral order below 33 K.⁹ Commensurate spiral spin ordering in Mn_3O_4 is described by an orthorhombic magnetic unit cell, which is twice the size of the chemical tetragonal unit cell.⁹ Magnon excitations in ferrimagnetic Mn_3O_4 have been recently investigated by Gleason *et al.*¹⁰ Magnetism in Mn_3O_4 couples to its dielectric properties. Consequently, dielectric anomalies are observed near the magnetic transition temperatures. In addition, magnetic field control of the dielectric constant below T_N has also been demonstrated.^{11,12}

While Jahn-Teller ordering yields a high temperature cubic-tetragonal distortion in Mn_3O_4 ,^{7,8} spin ordering drives further lattice distortions in this spinel.¹³ Kim *et al.* reported a transition from tetragonal to monoclinic symmetry in single crystal Mn_3O_4 at the commensurate spiral ordering temperature ($T \sim 33$ K) under zero applied fields.¹³ In a subsequent report, Kim and coauthors proposed that the low temperature structure of Mn_3O_4 is orthorhombic in the space group $Fddd$.¹⁴ Similarly, Chung *et al.* have recently reported orthorhombic instabilities in Mn_3O_4 .¹⁵ While these initial efforts clearly illustrate a structural transformation in ferrimagnetic Mn_3O_4 , the complete low-temperature structure of Mn_3O_4 remains unresolved and is the focus of the present work. Extensive studies of the magnetostructural phases of Mn_3O_4 by Kim and coauthors show that in the presence of large magnetic fields, the structural distortion occurs at higher temperatures in the incommensurate spiral magnetic phase. Remarkably, a spin disordered phase

can be stabilized in Mn_3O_4 near 0 K when intermediate fields are applied parallel to the (110) direction. Here, applied fields transverse to the magnetic ordering direction frustrate spin ordering resulting in disordered spins far below the magnetic ordering temperature.¹³ Kim *et al.* have also shown an increase in the Néel temperature under pressure to temperatures as high as 54 K.¹⁴

We present here, a complete description of the low-temperature nuclear structure of Mn_3O_4 finding that tetragonal $I4_1/amd$ and orthorhombic $Fddd$ phases coexist in ferrimagnetic Mn_3O_4 . The orthorhombic $Fddd$ phase is spontaneously nucleated at the Néel temperature and its phase fraction increases slightly, attaining a maximum of about 55% near 8 K. The evolution of the unit cell volume as a function of temperature indicates a distortion in both the tetragonal $I4_1/amd$ and orthorhombic $Fddd$ phases below 42 K. Distortions in both low temperature tetragonal and orthorhombic phases are corroborated by detailed studies of polyhedra distortions which show deformations in both of these phases. In the orthorhombic phase, MnO_6 octahedra show elongation of equatorial Mn-O bonds while the MnO_4 tetrahedra show a decrease in the Mn-O bond length. Conversely, the distorted tetragonal phase shows shortened Mn-O equatorial bonds in the MnO_6 octahedra and elongated Mn-O bonds in the MnO_4 tetrahedra. We examine the role of strain in stabilizing coexisting tetragonal and orthorhombic phases in ferrimagnetic Mn_3O_4 and make comparisons of the structural distortion of Mn_3O_4 to those of other magnetic spinels. The complexities in understanding the variations of structural deformations in magnetic spinels are highlighted. The complete structural description of this spinel is pivotal to unraveling the complex ground states of this material. These results necessitate a reinvestigation of the magnetic structure of Mn_3O_4 , which was resolved considering only the tetragonal nuclear structure below the Néel temperature.

II. METHODS

Polycrystalline Mn_3O_4 was prepared from a $\text{MnC}_2\text{O}_4 \cdot 2\text{H}_2\text{O}$ precursor. The oxalate was decomposed at 600 °C for 3 hrs. The precursor powder was then ground, pelletized, and annealed at 1000 °C for 24 hrs and water quenched. Variable-temperature (7.5 K – 450 K) high-resolution ($\delta Q/Q \leq 2 \times 10^{-4}$, $\lambda = 0.41394$ Å) synchrotron x-ray powder diffraction was performed at beamline 11BM of the Advanced Photon Source, Argonne National Laboratory and the ID31 beamline ($\lambda = 0.39985$ Å) of the European Synchrotron Radiation Facility. Variable temperature measurements were collected on heating with a temperature scan rate of 0.8 K/min and an x-ray pattern was collected every 3 minutes. Diffraction patterns were fit to crystallographic models using the EXPGUI/GSAS software program.^{16,17} Crystal structures were visualized using the program VESTA.¹⁸ Density measurements of a powder sample

of Mn_3O_4 were performed on a MicroMetrics AccuPyc II 1340 pycnometer. A sample cup with a volume of 0.1 cm^3 was filled with Mn_3O_4 powder with a mass of 93.1 mg during the density measurement. Temperature-dependent and field-dependent magnetic measurements were performed using the Quantum Design (QD) MPMS 5XL superconducting quantum interference device (SQUID). Heat capacity measurements were collected using a QD Physical Properties measurement system. Mn_3O_4 pellets for dielectric measurements were spark plasma sintered at 1000 °C under a 6 kN load for 3 minutes. Prior to measuring dielectric properties, the spark plasma sintered pellet was annealed at 1000 °C for 12 hrs, quenched, and characterized by x-ray diffraction to ensure that stoichiometric Mn_3O_4 was retained. Dielectric measurements were performed on a pellet with a diameter of 9.51 mm and a thickness of 2.28 mm whose cylindrical faces were coated by conducting epoxy. Dielectric properties were measured by an Andeen-Hagerling AH2700A capacitance bridge connected to the sample by shielded coaxial cables. The sample was placed in a QD Dynacool Physical Properties measurement system which provides a variable temperature and variable field environment when carrying out dielectric measurements.

III. RESULTS AND DISCUSSION

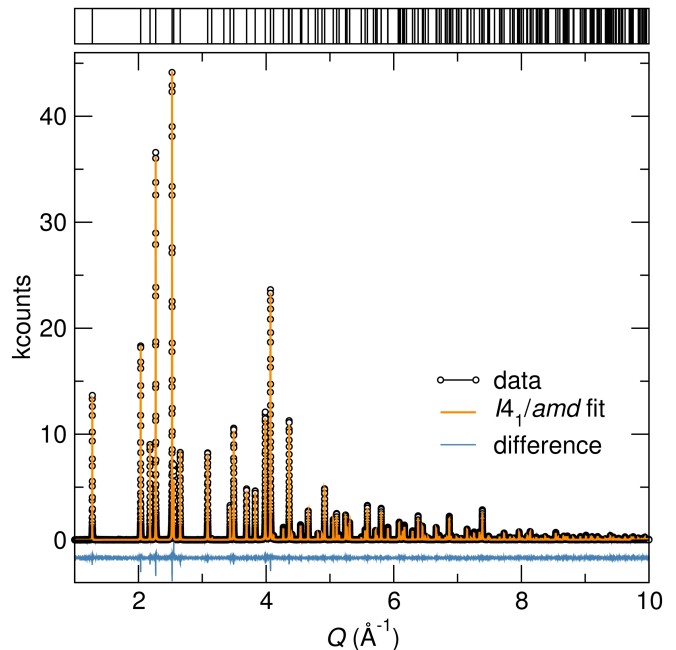


FIG. 1: (Color online) The room temperature synchrotron diffraction pattern of Mn_3O_4 modeled using the tetragonal $I4_1/amd$ structure.

At room temperature Mn_3O_4 is a tetragonal spinel in the space group $I4_1/amd$. The synchrotron x-ray

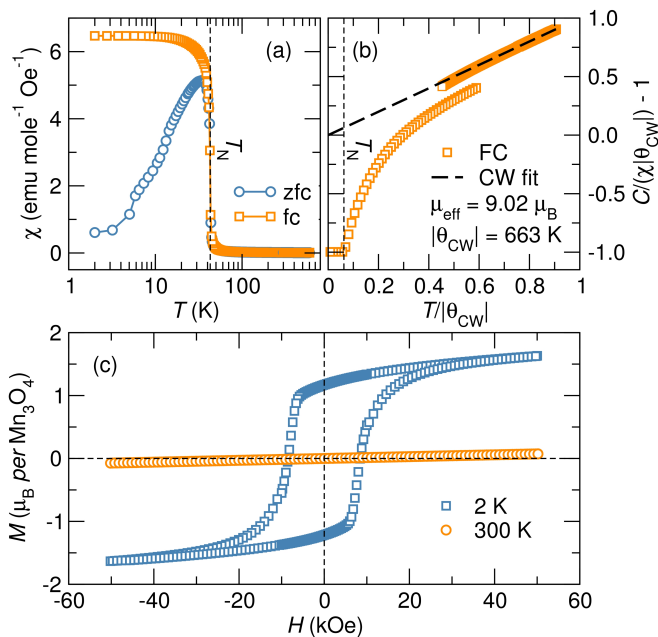


FIG. 2: (Color online) (a) Temperature dependent magnetic susceptibility measurements of Mn_3O_4 performed in a 1000 Oe field show a deviation of the zero-field cooled susceptibility from the field cooled susceptibility below the Néel temperature $T_N = 42$ K. (b) Curie-Weiss fitting in the temperature range $500 \text{ K} < T < 600 \text{ K}$ yields an effective moment of $9.02 \mu_B$ and an expected ordering temperature $|\Theta_{CW}| = 663 \text{ K}$. High-temperature and low-temperature susceptibility measurements were conducted on different instruments and instrumental variations yield the slight offset between the low-temperature and high-temperature susceptibility that is negligible in plot (a) but emphasized in the $1/\chi$ scaling of plot (b). (c) Field-dependent magnetization shows paramagnetic behavior above the Néel temperature of Mn_3O_4 and ferrimagnetic behavior below T_N with a saturation magnetization of $1.63 \mu_B$ and a coercive field of 8.5 kOe when $H = 50 \text{ kOe}$ and $T = 2 \text{ K}$.

diffraction pattern measured at 298 K and modeled to the space group $I4_1/amd$ is illustrated in fig. 1. Rietveld refinement of the diffraction pattern yields lattice constants $a = 5.76289(2) \text{ \AA}$ and $c = 9.46885(1) \text{ \AA}$ with a $c/a\sqrt{2}$ of 1.16 in good agreement with values from the literature.^{19,20} Goodness of fit parameters χ^2 , R_{wp} , and R_p of 2.354 , 10.23% , and 8.11% respectively are obtained from the refinement. Valence bond sums computed using room temperature bond lengths show that Mn_3O_4 is a normal spinel with tetrahedral and octahedral valence states of 2.01 and 3.02 respectively.

A broad transition from a paramagnetic to a ferrimagnetic state, which is characteristic of polycrystalline Mn_3O_4 ,¹¹ occurs near $T_N = 42 \text{ K}$. At T_N , a separation between the zero-field cooled and field cooled curves develops and is enhanced with decrease in temperature [fig. 2 (a)]. While a single broad magnetic transition is observed in the temperature-dependent susceptibility, the magnetic structure of Mn_3O_4 is extremely rich, featur-

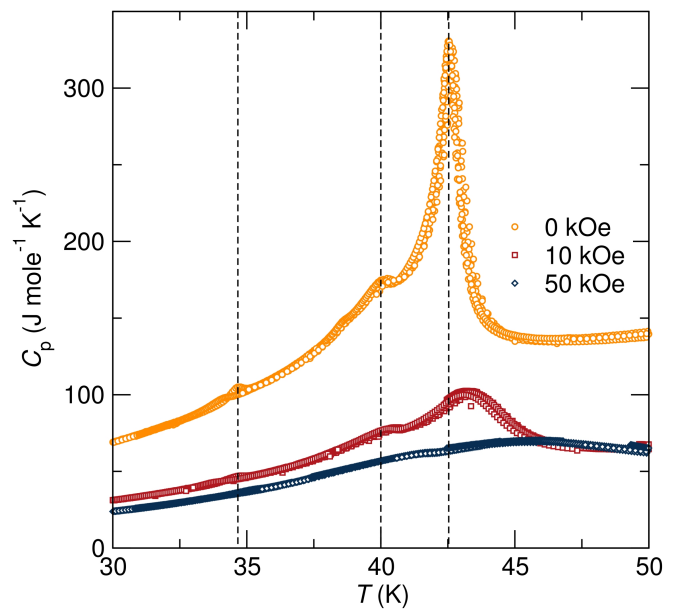


FIG. 3: (Color online) Heat capacity measurements of Mn_3O_4 show three anomalies associated with changes in magnetic structure at 42.5 K , 40 K , and 34.5 K . These transitions are evident under zero field conditions but they are suppressed and shifted to higher temperatures in the presence of a magnetic field.

ing a transition to a collinear magnetic structure at 42 K followed by the onset of an incommensurate magnetic spiral at 39 K , and finally a commensurate spiral magnetic state occurs below 33 K .^{9,21} Each of these transitions is observed in heat capacity and capacitance measurements as discussed later in the manuscript. Curie-Weiss fitting in the temperature range $500 \text{ K} < T < 600 \text{ K}$ yields a Θ_{CW} of 663 K in good agreement with prior work [fig. 2 (b)].^{20,21} Comparison between the expected Curie-Weiss ordering temperature and T_N results in a significant frustration index of 15.8 . This illustrates that frustration may play a role in the magnetism of Mn_3O_4 . The Curie-Weiss fit also yields an effective moment of $9.02 \mu_B$ which is congruent with the expected effective moment of $9.11 \mu_B$ computed from the spin-only effective moments of Mn^{2+} and Mn^{3+} which are $5.92 \mu_B$ and $4.9 \mu_B$ respectively. Short-range correlations cause deviations of the inverse susceptibility from the Curie-Weiss model above the Néel temperature as illustrated in fig.2 (b).

The weak linear increase in magnetization with field in the paramagnetic phase evolves to a hysteretic magnetization in ferrimagnetic Mn_3O_4 [fig. 2 (c)]. A saturation magnetization of $1.63 \mu_B$ and a coercive field of 8.5 kOe are measured at 50 kOe and 2 K . A collinear ferrimagnetic state in Mn_3O_4 would yield a saturation magnetization of $3 \mu_B/\text{formula unit}$, however, the measured saturation moment of $1.63 \mu_B$ is consistent with the reported spiral magnetic structure of Mn_3O_4 near 2 K .⁹ Mn_3O_4 exhibits significant anisotropy with an easy axis along the (001) direction, which yields a spontaneous magnetiza-

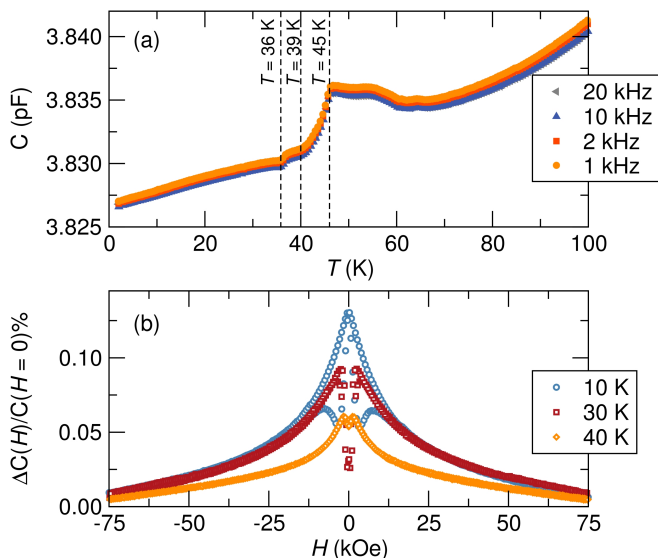


FIG. 4: (Color online) Magnetodielectric coupling in Mn_3O_4 . (a) The dielectric constant as a function of temperature shows three anomalies at 36 K, 39 K, and 45 K which are in close proximity to spin ordering transitions. (b) A magnetic field can modulate the dielectric constant below T_N . The changes in the dielectric constant in the presence of a magnetic field increase with decrease in temperature.

tion of $1.85 \mu_B$ in single crystalline samples.²² However, a slightly decreased value of the spontaneous magnetization is expected in polycrystalline materials due to the random alignment of Mn_3O_4 grains.^{11,22}

Spin ordering in Mn_3O_4 leads to changes in entropy that are illustrated in fig. 3. Variations in magnetic structure give rise to distinct heat capacity anomalies at 42.5 K, 40 K, and 34.5 K under zero-field conditions. The largest change in entropy occurs at 42 K where the highest heat capacity peak is observed. Entropy changes in Mn_3O_4 depend on the applied magnetic field, with large fields suppressing the heat capacity transitions. At 10 kOe field, heat capacity peaks are broad but still visible at the transition temperatures and the 42.5 K peak shifts to a higher temperature, $T_N = 43.2$ K. Pronounced suppression of the heat capacity transitions is evident at 50 kOe. The trend in the field-dependent heat capacity reported here, namely, the suppression of heat capacity anomalies and the shift to higher temperatures is in agreement with the work of Kim *et al.*, which reports an increase in T_N in the presence of a field and complete suppression of the onset of magnetic order when a magnetic field is applied along certain crystallographic directions.^{13,14}

Mn_3O_4 is a known magnetodielectric.^{11,12} Figure 4 (a) shows anomalies in the dielectric constant occurring in close proximity to spin ordering transition temperatures at 45 K, 39 K, and 36 K. The dielectric constant shows no frequency dependence and this illustrates the intrinsic nature of magnetodielectric coupling in the studied Mn_3O_4 sample. A frequency dependent dielectric

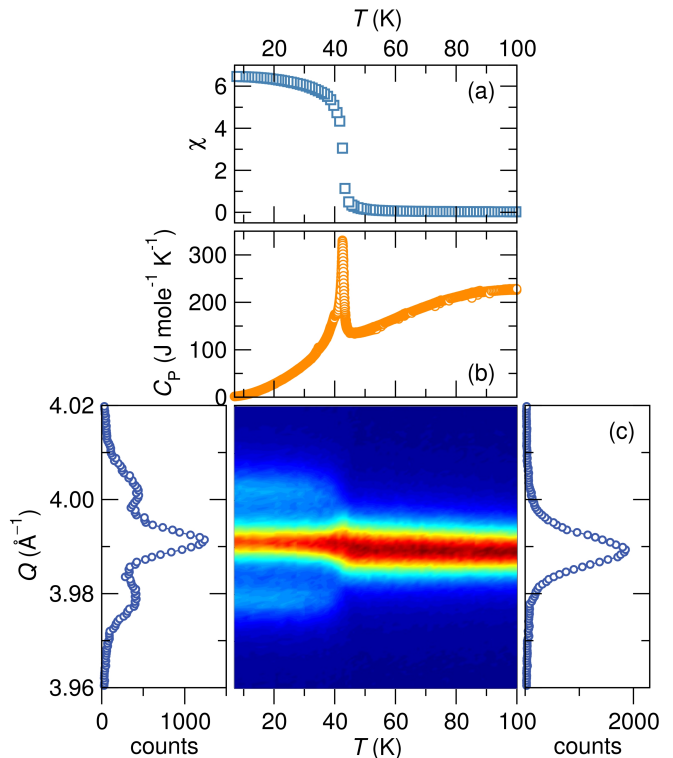


FIG. 5: (Color online) Concurrent magnetic and structural ordering in Mn_3O_4 . (a) Magnetic susceptibility measurements in units of $\text{emu mole}^{-1} \text{Oe}^{-1}$ and (b) heat capacity measurements show the onset of long-range ferrimagnetic order in Mn_3O_4 near 42 K. (c) A structural distortion occurs concomitantly with the onset of ferrimagnetic order in Mn_3O_4 at 42 K where variable-temperature high-resolution synchrotron x-ray diffraction shows a splitting of the high temperature tetragonal (321) reflection. While there is a decrease in intensity of the tetragonal (321) reflection in the low temperature phase, we note that it coexists with the emergent peaks to the lowest temperatures studied.

constant would indicate that magnetoresistive effects are contributing to magnetodielectric coupling. We also note the presence of dielectric anomalies above 45 K [fig 4 (a)], which could be linked to short-range spin correlations in the temperature range $T_N < T < |\Theta_{CW}|$. The origin of the dielectric changes above T_N should be further investigated. The dielectric constant exhibits strong field dependence below T_N [fig.4 (b)]. The field dependence of the dielectric constant increases with decrease in temperature.

The onset of long-range magnetic order in Mn_3O_4 occurs concurrently with a structural distortion. Figure 5 (a) and (b) show spin and entropy changes occurring concurrently near 42 K. Figure 5 (c) also shows x-ray diffraction evidence of structural changes in Mn_3O_4 occurring simultaneously near 42 K. A splitting of the tetragonal $I4_1/amd$ (321) reflection to several peaks below 42 K is clearly demonstrated by variable-temperature high-resolution synchrotron x-ray diffraction [Fig. 5 (c)]. The emergence of new diffraction peaks below 42 K indicates

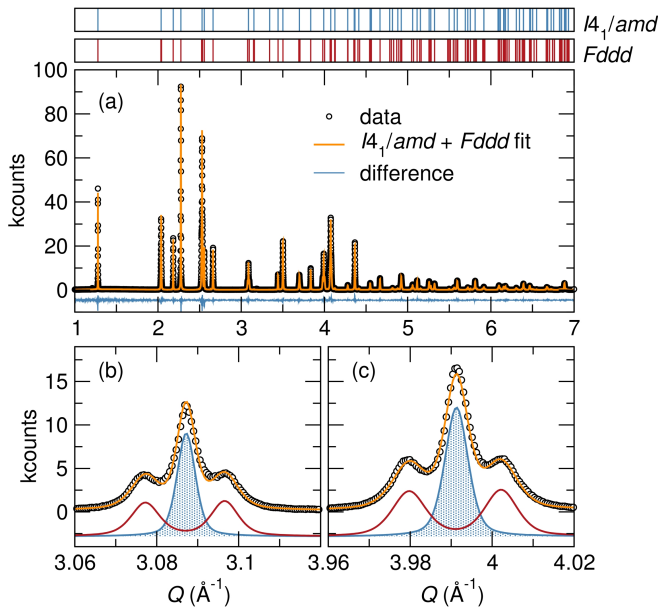


FIG. 6: (Color online) (a) The 8.2 K synchrotron x-ray diffraction pattern of Mn_3O_4 modeled to a structure of coexisting tetragonal $I4_1/amd$ and orthorhombic $Fddd$ structures. (b) The tetragonal $I4_1/amd$ (220) reflection splits into three reflections consisting of the tetragonal reflection and the orthorhombic $Fddd$ reflections (040) and (400). (c) In a similar way, tetragonal (321) reflection splits giving rise to the orthorhombic $Fddd$ (511) and (151) reflections.

an average structure distortion. This study of polycrystalline Mn_3O_4 shows that the magnetostructural distortion occurs near 42 K [fig. 5 (c)] while earlier studies of single crystal Mn_3O_4 have reported a 33 K magnetostructural distortion under zero-field conditions and a 39 K spin-drive structural transition in the presence of an applied magnetic field.^{13,14} The difference in the transition temperature is attributed to varying strain effects in polycrystalline versus single crystal samples; large strains in single crystal samples could suppress the onset of the structural transition. In addition, the cooling and heating rates of the sample during a structural study are also expected to influence the structural distortion temperature.

The precise structural description of Mn_3O_4 in the ferrimagnetic state is so far unknown. We find that Mn_3O_4 undergoes a phase transformation from tetragonal $I4_1/amd$ symmetry to a phase coexistence regime consisting of both tetragonal $I4_1/amd$ and orthorhombic $Fddd$ phases. Figure 6 (a) shows the 8.2 K diffraction pattern of Mn_3O_4 modeled by tetragonal $I4_1/amd$ and orthorhombic $Fddd$ phases. Structural parameters and goodness of fit parameters obtained from Rietveld refinement are tabulated in Table I. Small goodness of fit parameters along with the agreement between the model and the data illustrates that coexisting tetragonal and orthorhombic phases characterize ferrimagnetic Mn_3O_4 . No single phase low symmetry solution could

TABLE I: Structural parameters of coexisting tetragonal $I4_1/amd$ and orthorhombic $Fddd$ phases of Mn_3O_4 at 8.2 K.

Temperature (K)	8.2
Space group	$I4_1/amd$
Setting	origin 2
Z	4
a (Å)	5.75638(1)
c (Å)	9.44393(4)
Vol/(Å ³)	312.934(1)
Mn ²⁺	4a (0, 1/4, 7/8)
Mn ³⁺	8d (0, 1/2, 1/2)
O	16h (0, y, z)
	y 0.4715(2)
	z 0.2595(2)
Mn ²⁺ U_{iso} (10 ⁻² Å ²)	1.41(2)
Mn ³⁺ U_{iso} (10 ⁻² Å ²)	1.38(1)
O U_{iso} (10 ⁻² Å ²)	1.51(3)
Wt. frac.	0.44(6)
Space group	$Fddd$
Setting	origin 2
Z	8
a (Å)	8.11602(5)
b (Å)	8.16717(5)
c (Å)	9.44209(5)
Vol/(Å ³)	625.869(4)
Mn ²⁺	8a (1/8, 1/8, 1/8)
Mn ³⁺	16d (1/2, 1/2, 1/2)
O	32h (x, y, z)
	x 0.4871(2)
	y 0.4869(2)
	z 0.2585(2)
Mn ²⁺ U_{iso} (10 ⁻² Å ²)	1.25(2)
Mn ³⁺ U_{iso} (10 ⁻² Å ²)	1.21(2)
O U_{iso} (10 ⁻² Å ²)	1.45(3)
Wt. frac.	0.56(6)
χ^2	3.206
R_p (%)	5.46
R_{wp} (%)	6.82

be obtained to model the low temperature structure of Mn_3O_4 . A closer look at some of the diffraction reflections that split below the Néel temperature is presented in Fig. 6 (b) where the tetragonal (220) reflection coexists with orthorhombic (040) and (400) reflections. Similarly, fig. 6 (c) shows the coexistence of the tetragonal (321) and the orthorhombic (511) and (151) reflections. The orthorhombic $Fddd$ space group is a subgroup of the tetragonal space group $I4_1/amd$, and it has been shown to describe structural ground states of the Jahn-Teller active spinels NiCr_2O_4 and CuCr_2O_4 .²³ Magnetostructural phase transitions leading to complex structural ground states are an emerging theme in magnetic spinels; a re-

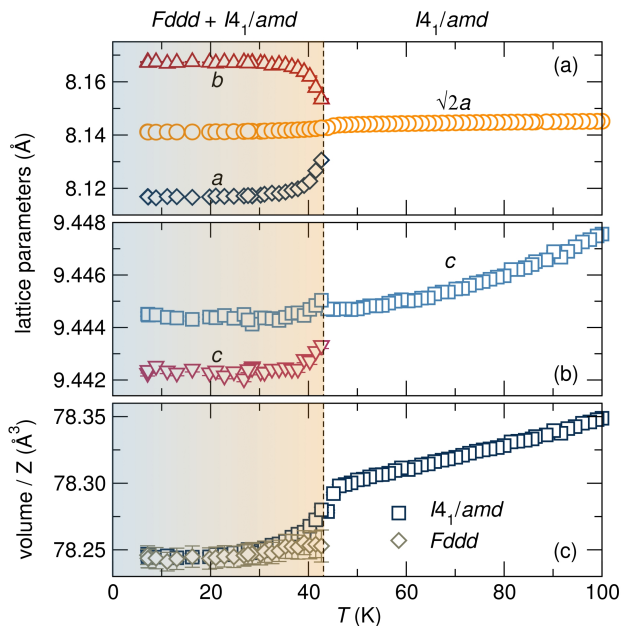


FIG. 7: (Color online) Temperature-dependence of the structural parameters of Mn_3O_4 . (a) Variation of the tetragonal a lattice constant of Mn_3O_4 with temperature shows the emergence of a compressed orthorhombic a lattice constant and an elongated orthorhombic b lattice constants below 42 K. (b) The tetragonal c lattice constant decreases with temperature to 42 K, below which the orthorhombic c lattice constant, which has a decreased value, emerges. (c) A linear decrease in the unit cell volume is observed above 42 K. At 42 K, a discontinuous decrease in cell volume is observed in both the tetragonal $I4_1/amd$ and orthorhombic $Fddd$ phases.

cent report from our group shows structural phase coexistence in MgCr_2O_4 and ZnCr_2O_4 .²⁴

The low-temperature structures coexist with nearly equal fractions below T_N . Weight fractions of 50.4% and 49.6% for the $I4_1/amd$ and $Fddd$ phases respectively are measured near T_N . With decrease in temperature below T_N , the orthorhombic phase fraction increases slightly attaining a maximum value of 56% near 8 K. Scherrer analysis reveals that large crystallite sizes with dimensions $> 10\mu\text{m}$ are observed in the high temperature and low temperature tetragonal phases while smaller domain sizes of about 690 nm characterize the orthorhombic phase. The simple Scherrer model of crystallite size analysis neglects instrumental broadening, therefore, the sizes obtained are the minimum values.

At the magnetostructural ordering temperature of Mn_3O_4 , orthorhombic $Fddd$ lattice constants emerge and coexist with tetragonal $I4_1/amd$ lattice constants (Fig. 7). The orthorhombic a and b lattice constants derive from the tetragonal a lattice parameter. A $\approx 0.3\%$ compression of the orthorhombic a axis and a $\approx 0.33\%$ elongation of the orthorhombic b axis relative to the tetragonal a lattice constant are measured [Fig. 7 (a)]. The continuous decrease of the tetragonal c axis that occurs above 42 K, is disrupted at T_N where the orthorhombic

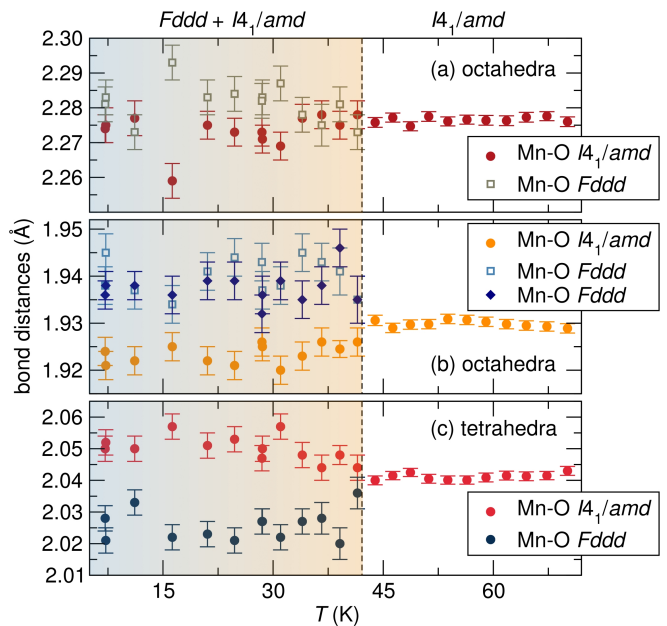


FIG. 8: (Color online) Polyhedra distortions of Mn_3O_4 . (a) The axial Mn-O bond length of the MnO_6 octahedra shows relative temperature independence across the structural phase transition in both the tetragonal and orthorhombic phases. (b) The equatorial Mn-O bond length of MnO_6 octahedra in the high temperature tetragonal phase has a value of about 1.93 Å. Below the structural phase transition, this equatorial bond length is compressed in the tetragonal phase and has a value of ≈ 1.92 Å. In the orthorhombic phase, this bond length is distorted giving rise to two different equatorial bonds with lengths of about 1.94 Å. (c) Below T_N , the Mn-O bond length of the MnO_4 polyhedra increases in length in the tetragonal phase while its length decreases in the orthorhombic phase.

c axis emerges with values $\approx 0.02\%$ smaller relative to the tetragonal c axis [Fig. 7 (b)]. The temperature-dependence of the unit cell volume shows a discontinuous decrease below 42 K [Fig. 7 (c)]. In the Ehrenfest classification of phase transitions, first order phase transitions are characterized by a discontinuous change in the first derivative of the free energy. The discontinuous change in the cell volume of Mn_3O_4 and coexistence of two low-temperature structures suggests that this is a first order phase transition. The structural distortion of Mn_3O_4 , $b_{orth}/a_{tet}=1.003$, is of the same order as those of other spin driven lattice distortions observed in the related spinel compounds NiCr_2O_4 ,²³ CuCr_2O_4 ,²³ ZnCr_2O_4 ,²⁴ and MgCr_2O_4 .²⁴

The complete crystallographic description of Mn_3O_4 enables detailed investigation of polyhedral distortions that occur following the structural distortion. The elongated MnO_6 polyhedral units of tetragonal Mn_3O_4 above T_N are described by an apical bond length of 2.275(9) Å, which is twofold degenerate and an equatorial bond length of 1.93(3) Å that is fourfold degenerate [Fig. 8 (a) and (b)]. Below the structural transition temperature, the apical bond length remains fairly tem-

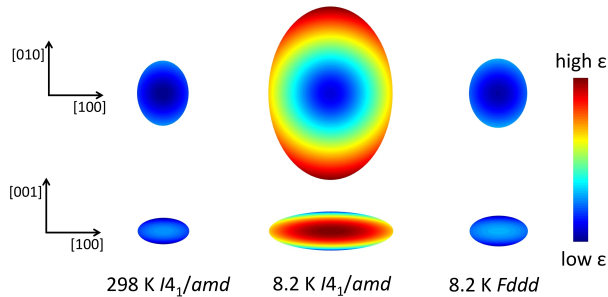


FIG. 9: (Color online) Ellipsoid representation of the second rank strain tensor of Mn_3O_4 in the various phases as determined by Rietveld refinement using the Pseudo-Voigt with Finger-Cox-Jephcoat asymmetry (GSAS profile 3) profile function. In addition to the color scale, the size of the ellipsoid scales with the magnitude of the strain. In all the phases of Mn_3O_4 , large strains are observed in the $[110]$ plane compared to the $[001]$ direction. The low temperature tetragonal $I4_1/amd$ phase is highly strained compared to the high temperature tetragonal phase and low temperature orthorhombic phase. The high temperature $I4_1/amd$ phase shows the lowest strains of the three phases of Mn_3O_4 .

perature independent with small variations around the $2.275(5)$ Å value in both the tetragonal and orthorhombic phases [Fig. 8 (a)]. On the other hand, below T_N , the equatorial bond length of the tetragonal phase decreases to a length of about $1.92(5)$ Å while retaining its fourfold degeneracy. The equatorial Mn-O bond length of MnO_6 octahedra exhibits distortions in the orthorhombic phase that yield two Mn-O bond lengths that are about $1.935(5)$ Å long, each with twofold degeneracy [Fig. 8 (b)]. The high temperature tetragonal phase has a tetrahedral Mn-O bond length of 2.04 Å, this bond length increases to $\approx 2.05(3)$ Å in the low temperature tetragonal phase while it decreases in the orthorhombic phase to $\approx 2.025(4)$ Å [Fig. 8 (c)]. The distortions of the polyhedra in each of the low temperature structures are complementary, for instance examining the low temperature orthorhombic phase: the elongation of the equatorial bond lengths of MnO_6 octahedra are compensated by the decrease in Mn-O bond lengths of the MnO_4 tetrahedra.

High resolution synchrotron x-ray diffraction has emerged as an important tool for characterizing the low temperature structures of magnetic materials.^{5,23,24} However, it has been shown that chemical inhomogeneity that is present at all times, but cannot be easily detected by high resolution x-ray diffraction above the phase transition temperature, can lead to structural phase coexistence below a structural phase transition temperature.⁵ In this light, we have refined the elemental occupancies of all atoms in the low temperature tetragonal and orthorhombic phases. All elements remain stoichiometric within error. The highest vacancy concentration of 1.33% is obtained for Mn^{3+} cations in the orthorhombic phase. Nevertheless, this small vacancy concentration cannot account for $> 50\%$ orthorhombic phase content

TABLE II: Microstrain terms of the various phases of Mn_3O_4 obtained from Rietveld refinement. The magnitude of the microstrain terms of the low temperature tetragonal phase are larger than those of the other phases of Mn_3O_4 . These strain tensors have been plotted in an ellipsoidal representation in Fig 9. Pseudo-Voigt profile with Finger-Cox-Jephcoat asymmetry was employed in describing the diffraction lineshapes.

Microstrain term	298 K $I4_1/amd$	8.2 K $I4_1/amd$	8.2 K $Fddd$
L_{11}	0.1071	-0.0257	0.1666
L_{22}	0.159	-0.3624	0.1975
L_{33}	0.0743	0.1071	0.0837
L_{12}	0.1093	0.3676	-0.0481
L_{13}	-0.0151	-0.0392	-0.0127
L_{23}	-0.0218	-0.02115	-0.0350

observed below T_N . We have performed high-precision density measurements of the Mn_3O_4 sample to further investigate the stoichiometry of this material. Density measurements of the powder sample at room temperature give a density of $4.855(9)$ g/cm³ which compares well with the expected density of 4.86 g/cm³ confirming that off-stoichiometric effects are not influencing the structural phase transition of this sample.

Structural phase coexistence in Mn_3O_4 is linked to large strains at the phase transition temperature due to the lattice mismatch between the low temperature orthorhombic phase and the high temperature tetragonal phase. Figure. 7 shows that the orthorhombic a and b lattice constants vary by 0.3% from those of both the high temperature and low temperature tetragonal phases. The c axis varies slightly, by 0.02% between the $Fddd$ and $I4_1/amd$ phases. The map of the strain tensor shows a highly strained low temperature tetragonal phase (Fig. 9). Most of the strain is along the crystallographic a and b axes where the largest lattice mismatch between the low temperature tetragonal and orthorhombic phases is observed. The orthorhombic $Fddd$ phase also experiences slightly higher strain compared to the high temperature tetragonal phase. It is important to note the significantly smaller strain along the $[001]$ direction, this finding agrees well with the fairly invariant c lattice constants of the high temperature and low temperature phases. Evidence of strain stabilized structural phase coexistence in Mn_3O_4 is corroborated by the work of Suzuki and Katsufuji, who have performed strain measurements on single crystals of Mn_3O_4 observing changes in the temperature dependent strain ($\Delta L/L$) at the magnetic ordering temperatures.¹² Suzuki and Katsufuji also show larger strain effects along the $[110]$ plane of Mn_3O_4 compared to the $[001]$ direction.¹²

Evidence of coexisting tetragonal and orthorhombic phases is in agreement with prior studies of the hausmanite Mn_3O_4 . Chung *et al.* reported orthorhombic instabilities in a single crystal of Mn_3O_4 after observing subtle diffraction peak asymmetry.¹⁵ The study by Chung *et al.* essentially indicates the present of coexisting phases in

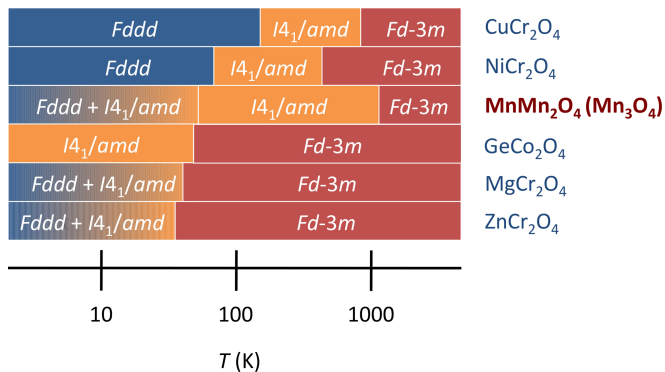


FIG. 10: (Color online) Structural distortions in some spinels due to Jahn-Teller ordering and magnetostructural coupling effects. While in many instances full structural transformations occur, phase coexistence is observed for MgCr_2O_4 , ZnCr_2O_4 , and Mn_3O_4 .

Mn_3O_4 below T_N , with the tetragonal phase yielding dominant peaks and the orthorhombic phase contributing to mere peak asymmetry. Considering the work of Chung and coworkers, it is clear that large strains in a single crystal can inhibit the formation of a large phase fraction of the low temperature orthorhombic phase. The polycrystalline sample examined here along with the use of high-resolution synchrotron x-ray diffraction allows us to fully resolve the diffraction reflections of the orthorhombic $Fddd$ phase and to complete a detailed study of the structural changes taking place at low temperatures.

The structural phase transformation of Mn_3O_4 bears some of the hallmark characteristics of a martensitic phase transformation. We observe the nucleation of an orthorhombic $Fddd$ phase within the matrix of the parent I_{41}/amd phase. Strain energy inhibits the complete structural transformation of Mn_3O_4 to the orthorhombic phase, stabilizing a mixed phase structure. Comparable strain-mediated structural phase coexistence is reported in the manganites $\text{Bi}_{0.2}\text{Ca}_{0.8}\text{MnO}_3$ and $\text{La}_{0.275}\text{Pr}_{0.35}\text{Ca}_{0.375}\text{MnO}_3$.²⁵ However, it must be noted that the perovskites are usually on the verge of being metals and the inhomogeneities are frequently the result of very slightly differing levels of chemical doping, but this is not the case in Mn_3O_4 because it is stoichiometric and insulating. Examination of hysteresis effects of the structural phase transition of Mn_3O_4 are inconclusive due to slow heating and cooling rates applied during variable temperature x-ray measurements. A comparison of the magnetostructural phase transformation of Mn_3O_4 to spin-driven lattice deformations of other magnetic spinels suggests that phase coexistence likely occurs when structural deformations occur at low temperatures ($T < 50$ K) (Fig. 10). However, the spinel GeCo_2O_4 shows a full transformation from cubic to tetragonal symmetry near 22 K indicating that low temperatures do

not necessarily limit full structural transformations in all spinels and perhaps the particular strains involved in the lattice deformation play a larger role in stabilizing phase coexistence.

These results call for a re-examination of the properties of Mn_3O_4 at low temperatures. For example, how do we understand spin ordering in the various low temperature phases? Further, it is important to resolve the magnetic structure of Mn_3O_4 taking into account structural phase coexistence in the ferrimagnetic phase. Since strain influences phase coexistence, it presents a new approach to controlling the magnetostructural phase transition of Mn_3O_4 to achieve a desired low temperature structure.

IV. CONCLUSIONS

High resolution synchrotron x-ray diffraction reveals the coexistence of tetragonal I_{41}/amd and orthorhombic $Fddd$ below the Néel temperature of the magnetodielectric spinel Mn_3O_4 . The two low temperature phases coexist in nearly equal fractions. A complete crystallographic description of Mn_3O_4 in the ferrimagnetic state is presented. Polyhedral distortions in the ferrimagnetic phase of Mn_3O_4 are described. We show that strains due to the lattice mismatch between the orthorhombic phase, which is nucleated below 42 K, and the high temperature tetragonal I_{41}/amd phase likely contribute to the observed phase coexistence. We propose strain as a new approach to control the properties of Mn_3O_4 below the magnetic ordering temperature.

A. Acknowledgements

We thank Professor Van der Ven for helpful discussions. This project was supported by the NSF through the DMR 1105301. MCK is supported by the Schlumberger Foundation Faculty for the Future fellowship. We acknowledge the use of MRL Central Facilities which are supported by the MRSEC Program of the NSF under Award No. DMR 1121053; a member of the NSF-funded Materials Research Facilities Network (www.mrfln.org). Use of data from the 11-BM beamline at the Advanced Photon Source was supported by the U.S. Department of Energy, Office of Science, Office of Basic Energy Sciences, under Contract No. DE-AC02-06CH11357. Data were also collected on the ID31 beamline at the European Synchrotron Radiation Facility (ESRF), Grenoble, France. We thank Andy Fitch and Caroline Curfs for providing assistance in using beamline ID31. We thank Michael Gaultois, Quantum Design staff scientists Dr. Neil Dilley and Dr. Shi Li, and Quantum Design for high temperature susceptibility measurements.

-
- * Electronic address: kemei@mrl.ucsb.edu
† Electronic address: jkharada@mrl.ucsb.edu
‡ Electronic address: seshadri@mrl.ucsb.edu
§ Electronic address: suchomel@aps.anl.gov
- ¹ S. Jin, T. H. Tiefell, M. McCormack, R. A. Fastnacht, R. Ramesh, and L. H. Chen, *Science* **264**, 413 (1994).
 - ² M. Fth, S. Freisem, A. A. Menovsky, Y. Tomioka, J. Aarts, and J. A. Mydosh, *Science* **285**, 1540 (1999).
 - ³ M. Uehara, S. Mori, C. H. Chen, and S.-W. Cheong, *Nature* **399**, 560 (1999).
 - ⁴ K. H. Ahn, T. Lookman, and A. R. Bishop, *Nature* **428**, 401 (2004).
 - ⁵ A. Llobet, C. Frontera, J. L. Garcia-Munoz, C. Ritter, and M. A. G. Aranda, *Chem. Mater.* **12**, 3648 (2000).
 - ⁶ H. Y. Hwang, S.-W. Cheong, P. G. Radaelli, M. Marezio, and B. Batlogg, *Phys. Rev. Lett.* **75**, 914 (1995).
 - ⁷ J. B. Goodenough and A. L. Loeb, *Phys. Rev.* **98**, 391 (1955).
 - ⁸ H. J. van Hook and M. L. Keith, *Am. Mineral* **43**, 69 (1958).
 - ⁹ G. B. Jensen and O. V. Nielsen, *J. Phys. C: Solid State Phys.* **7**, 409 (1975).
 - ¹⁰ S. L. Gleason, T. Byrum, Y. Gim, A. Thaler, P. Abbamonte, G. J. MacDougall, L. W. Martin, H. D. Zhou, and S. L. Cooper, *Phys. Rev. B* **89**, 134402 (2014).
 - ¹¹ R. Tackett, G. Lawes, B. C. Melot, M. Grossman, E. S. Toberer, and R. Seshadri, *Phys. Rev. B* **76**, 024409 (2007).
 - ¹² T. Suzuki and T. Katsufuji, *Phys. Rev. B* **77**, 220402(R) (2008).
 - ¹³ M. Kim, X. M. Chen, Y. I. Joe, E. Fradkin, P. Abbamonte, and S. L. Cooper, *Phys. Rev. Lett.* **104**, 136402 (2010).
 - ¹⁴ M. Kim, X. M. Chen, X. Wang, C. S. Nelson, R. Budakian, P. Abbamonte, and S. L. Cooper, *Phys. Rev. B* **84**, 174424 (2011).
 - ¹⁵ J.-H. Chung, K. H. Lee, Y.-S. Song, T. Suzuki, and T. Katsufuji, *J. Phys. Soc. Jpn.* **82**, 034707 (2013).
 - ¹⁶ B. H. Toby, *J. Appl. Crystallogr.* **34**, 210 (2001).
 - ¹⁷ A. C. Larson and R. B. V. Dreele, Los Alamos National Laboratory Report pp. 86–748 (2000).
 - ¹⁸ K. Momma and F. Izumi, *J. Appl. Crystallogr.* **41**, 653 (2008).
 - ¹⁹ D. P. Shoemaker, E. E. Rodriguez, R. Seshadri, I. S. Abumohor, and T. Proffen, *Phys. Rev. B* **80**, 144422 (2009).
 - ²⁰ B. Chardon and F. Vigneron, *J. Magn. Magn. Mater.* **58**, 128 (1986).
 - ²¹ B. Boucher, R. Buhl, and M. Perrin, *J. Phys. Chem. Solids* **32**, 2429 (1971).
 - ²² B. Chardon and F. Vigneron, *Phys. Rev.* **119**, 1470 (1960).
 - ²³ M. R. Suchomel, D. P. Shoemaker, L. Ribaud, M. C. Kemei, and R. Seshadri, *Phys. Rev. B* **86**, 054406 (2012).
 - ²⁴ M. C. Kemei, P. T. Barton, S. L. Moffitt, M. W. Gaultois, J. A. Kurzman, R. Seshadri, M. R. Suchomel, and Y. Kim, *J. Phys.: Condens. Matter* **25**, 326001 (2013).
 - ²⁵ V. Podzorov, B. G. Kim, V. Kiryukhin, M. E. Gershenson, and S.-W. Cheong, *Phys. Rev. B* **64**, 140406(R) (2001).